# JMR Abstracts

Editor-in-Chief: Robert P. Frankenthal • Associate Editors: Shigeyuki Sōmiya, Heinrich J. Wollenberger

*Volume 14, Number 7* — *Abstracts for July 1999 Journal of Materials Research*


## TABLE OF CONTENTS

**Structural characterization of laser-ablated epitaxial $(Ba_{0.5}Sr_{0.5})TiO_3$ thin films on MgO(001) by synchrotron x-ray scattering**
S. Kim, T.S. Kang, J.H. Je

**Growth of graphite nanofibers from the decomposition of $CO/H_2$ over silica-supported iron–nickel particles**
P.E. Anderson, N.M. Rodriguez

**Kinetics and mechanism of anatase-to-rutile phase transformation in the presence of borosilicate glass**
J-H. Jean, S-C. Lin

**Equilibrium phases in Mn–V–O system under ambient atmosphere**
S.K. Chung, A.A. Andriiko, P.V. Rudenok, S.J. Shin

**Solution deposition processing and electrical properties of $Ba(Ti_{1-x}Sn_x)O_3$ thin films**
K.H. Yoon, J.H. Park, J.H. Jang

**Crack tip 90° domain switching in tetragonal lanthanum-modified lead zirconate titanate under an electric field**
F. Fang, W. Yang, T. Zhu

**Thermally induced structural changes in epitaxial $SrZrO_3$ films on $SrTiO_3$**
P.A. Langjahr, T. Wagner, M. Rühle, F.F. Lange

**Nucleation mechanisms in chemically vapor deposited mullite coatings on SiC**
P. Hou, S.N. Basu, V.K. Sarin

**Transmission electron microscopy observation of second-phase particles in β–$Si_3N_4$ grains**
N. Hirosaki, T. Saito, F. Munakata, Y. Akimune, Y. Ikuhara

**Microstructure in silicon nitride containing β-phase seeding**
H-H. Lu, J-L. Huang

**Origin of strength change in ceramics associated with the alteration of spray dryer**
T. Hotta, K. Nakahira, M. Naito, N. Shinohara, M. Okumiya, K. Uematsu

**Formation and characterization of hydroxyapatite coating layer on Ti-based metal implant by electron-beam deposition**
J-M. Choi, Y-M. Kong, S. Kim, H-E. Kim, C.S. Hwang, I-S. Lee

**Bismuth composition control of $SrBi_2TaNbO_9$ thin films by heat treating $Bi_2O_3$-inserted heterostructure**
Y-B. Park, J-K. Lee, H-J. Jung, J-W. Park

**Design for high-performance functional composite thermistor materials by glass/ceramic composing**
D.J. Wang, J. Qiu, Z.L. Gui, L.T. Li

**The morphology and growth mechanism of alumina whiskers in aluminum-based metal matrix composites**
Y-F. Li, C-D. Qin, D.H.L. Ng

**Powder synthesis of barium titanate and barium orthotitanate via an ethylene glycol complex polymerization route**
S.J. Lee, M.D. Biegalski, W.M. Kriven

**Quantitative adhesion measures of multilayer films: Part I. Indentation mechanics**
M.D. Kriese, N.R. Moody, W.W. Gerberich

**Quantitative adhesion measures of multilayer films: Part II. Indentation of W/Cu, W/W, Cr/W**
M.D. Kriese, N.R. Moody, W.W. Gerberich

**Phase evolution in Ni–Nb multilayers upon solid-state reaction**
G.W. Yang, C. Lin, B.X. Liu

**The role of the dispersed phase remnant magnetization on the redispersibility of magnetorheological fluids**
P.P. Phulé, M.P. Mihalcin, S. Genc

**Fabrication and properties of organic and metal nanocylinders in nanoporous membranes**
L. Piraux, S. Dubois, J.L. Duvail, A. Radulescu, S. Demoustier-Champagne, E. Ferain, R. Legras

**Oxidation kinetics of large nickel particles**
R. Karmhag, G.A. Niklasson, M. Nygren

**Influence of additives on the properties of spherical nickel particles prepared by ultrasonic spray pyrolysis**
S. Stopić, J. Nedeljković, Z. Rakočević, D. Uskoković

**Magnetic properties of uniform γ–$Fe_2O_3$ nanoparticles smaller than 5 nm prepared by laser pyrolysis**
M.P. Morales, S. Veintemillas-Verdaguer, C.J. Serna

**Preparation of phase homogeneous Mn–Zn ferrite powder by spray pyrolysis**
X. Zhao, B. Zheng, H. Gu, C. Li, S.C. Zhang, P.D. Ownby

**Electromechanical anisotropy behavior in $Pb_{0.88}Eu_{0.88}Ti_{1-y}Mn_yO_3$ system: Role of 90° domain reversal**
O. Pérez Martínez, J.M. Saniger Blesa, A. Peláiz Barranco, F. Calderón Piñar

**Preparation of epitaxial $SrBi_2Nb_2O_9$ and $SrBi_2Ta_2O_9$ thin films by coating-pyrolysis process**
T. Nagahama, T. Manabe, I. Yamaguchi, T. Kumagai, T. Tsuchiya, S. Mizuta

**Scanning electron acoustic microscopy of electric domains in ferroelectric materials**
M.L. Qian, X.M. Wu, Q.R. Yin, B.Y. Zhang, J.H. Cantrell

**Synthesis, electrochemical, and microstructural study of precursor-derived $LiMn_2O_4$ powders**
Y.H. Ikuhara, Y. Iwamoto, K. Kikuta, S. Hirano

**Eu-doped $Y_2O_3$ phosphor films produced by electrostatic assisted chemical vapor deposition**
K.L. Choy, J.P. Feist, A.L. Heyes, B. Su

**Influence of heat treatment on $LiNbO_3$ thin films prepared on Si (111) by the polymeric precursor method**
V. Bouquet, J.A. Varela, E. Longo, E.R. Leite

**Planar waveguides prepared by $K^+$–$Na^+$ field-assisted ion exchange in different types of silicate glass**
J. Kosíková, J. Schröfel

**$C_{24}Cs$ samples containing oriented $N_2$ molecules**
Y. Finkelstein, R. Moreh, D. Nemirovsky, O. Shahal, F. Beguin, L. Duclaux

**Structural mechanisms underlying near-zero thermal expansion in β-eucryptite: A combined synchrotron x-ray and neutron Rietveld analysis**
H. Xu, P.J. Heaney, D.M. Yates, R.B. Von Dreele, M.A. Bourke

**Effects of carbonization atmosphere and subsequent oxidation on pore structure of carbon spheres observed by scanning tunneling microscopy**
M. Inagaki, V. Vignal, H. Konno, A.W. Morawski

**Thin films with nanometer scale pillar microstructure**
K. Robbie, C. Shafai, M.J. Brett

**On the grain size and coalescence stress resulting from nucleation and growth processes during formation of polycrystalline thin films**
C.V. Thompson

**Microtexture of shock reaction products of niobium and silica mixtures**
R. Murao, M. Kikuchi, K. Fukuoka, E. Aoyagi, T. Atou, Y. Syono

# ABSTRACTS

## RAPID COMMUNICATIONS

### Magnetic properties of $Tb_2(Fe,Si)_{17}$ single crystals

Y.X. Li, S.X. Gao, J. Du, C.C. Tang, C. Cai, G.H. Wu, W.S. Zhan
*(Chinese Academy of Sciences)*

The magnetic properties of single-crystalline $Tb_2Fe_{17-x}Si_x$ ($x$ = 0, 1, 2, 3, and 3.3) have been investigated. The Si substitution constricted the lattices by 1.5% and caused the $Th_2Ni_{17}$ transfer to $Th_2Zn_{17}$. The Curie temperature increased from 413 to 526 K, and the spontaneous magnetic moment decreased from 82.6 to 46.4 emu/g with the increase of Si. The stronger anisotropy and coercivity were generated by Si occupying the Fe sublattices. A domain wall pinning-dominated mechanism was responsible for increasing the coercivity force from 0.01 T ($x$ = 1) to about 0.36 T ($x$ = 3.3) at 1.5 K.

**Order No.: JA907-001** 

### Sintering behavior of nanophase $MoSi_2$ with and without a $ZrO_2$ additive

Q. Tan, A. Zangvil
*(University of Illinois—Urbana-Champaign)*

It was shown that sintering temperature could be lowered and the density, hardness, and toughness of $MoSi_2$ raised by using nanophase $MoSi_2$ and $ZrO_2$ additives. A minimum hot-pressing temperature of 1350 °C was needed for complete densification without a significant increase in grain size.

**Order No.: JA907-002** 

### Microstructural characteristics of TiC-reinforced composite coating produced by laser syntheses

X. Wu
*(Chinese Academy of Sciences)*

An *in situ* method has been developed to produce a Ni alloy composite coating reinforced by *in situ* reacted and gradiently distributed TiC particles by one-step laser cladding. The dispersed, ultrafine TiC particles in the coating were observed. Most of the TiC particles, with an evidently gradient distribution, were uniformly distributed within interdendritic regions due to the trapping effect of advanced solid–liquid interface. The TiC/γ–Ni interface was clean and free from deleterious surface reactions. The microhardness of the coating also had a gradient variation, with the highest value being 1250 Hv 0.2.

**Order No.: JA907-003** 

### The early stages of oxidation of aluminum nitride

Y. Geng, M.G. Norton
*(Washington State University)*

The early stages of oxidation of aluminum nitride have been studied using transmission electron microscopy and electron diffraction. It was found that the oxide layer grew by the Stranki–Krastonow mechanism, where an initial uniform layer was followed by island formation. The onset of oxidation occured at 800 °C, and the initial oxide phase that formed was γ–$Al_2O_3$, one of the transition aluminas. The orientation relationship between the oxide layer and the underlying nitride is $(440)_\gamma \| (11\bar{2}0)_{AlN}$ and $[\bar{1}12]_\gamma \| [01\bar{1}0]_{AlN}$.

**Order No.: JA907-004** 

### Preparation of highly oriented $Pb(Zr_{0.52}Ti_{0.48})O_3$ thin films by sol-gel hydrothermal process

J. Zeng[1], C. Lin[1], J. Li[2], K. Li[2]
*([1]Chinese Academy of Sciences, [2]Jiangsu Institute of Petrochemical Technology)*

A novel sol-gel-hydrothermal process for the preparation of highly oriented thin films of $Pb(Zr_{0.52}Ti_{0.48})O_3$ is reported. $Pb(Zr_{0.52}Ti_{0.48})O_3$ thin films with fully (111) orientation were successfully prepared on platinized silicon substrates at low temperature (100–200 °C) by combining a conventional sol-gel process and hydrothermal method, i.e., sol-gel-hydrothermal technique. The x-ray rocking curve for the (111) reflection as measured by high-resolution four-crystal diffractometer showed a narrow full width at half-maximum value of 0.20° for the as-prepared films. A dense, pinhole-free, uniform surface morphology was observed from atomic force microscopy images of the films. The low leakage current density of the prepared films was also found.

**Order No.: JA907-005** 

## REVIEW

### InGaN/GaN/AlGaN-based laser diodes grown on epitaxially laterally overgrown GaN

S. Nakamura
*(Nichia Chemical Industries, Ltd.)*

Epitaxially laterally overgrown GaN on sapphire was used to reduce the number of threading dislocations originating from the interface of the GaN epilayer with the sapphire substrate. The GaN layer above the $SiO_2$ mask area surrounding the window and corresponding to the lateral overgrowth was nearly free of threading dislocations. A high density of threading dislocations was observed in the vicinity of GaN grown in the window regions. InGaN multiquantum-well-structure laser diodes (LDs) grown on pure GaN substrates, which were fabricated by removing the sapphire substrate, were demonstrated. The LDs with output power of 5 mW exhibited a lifetime of more than 290 h and an estimated lifetime of 10,000 hours despite a relatively large threshold current density. The far-field pattern of the LDs with a cleaved mirror facet revealed single-mode emission without any interference effects.

**Order No.: JA907-006** 

## ARTICLES

### High-resolution electron microscopy investigations of stacking faults in $Y_1Ba_2Cu_3O_{7-\delta}$ metalorganic chemical vapor deposited thin films

Ch. Grigis, S. Schamm, D. Dorignac
*(CEMES/CNRS)*

New structural planar defects in Ba-deficient ($Y_1Ba_2Cu_3O_{7-\delta}$ 1 : 1.6 : 3) thin films grown on $NdGaO_3$ and $SrTiO_3$ substrates by metalorganic chemical vapor deposition have been observed by means of high-resolution electron microscopy. The defects are associated with perturbations of the YBCO "1 : 2 : 3" stacking sequences along the $c$ direction, which give rise to structural variants having locally "2 : 5 : 7," "3 : 4 : 7," or "4 : 6 : 10" cationic stoichiometries. The defects can be consistently interpreted as CuO–YO–CuO/CuO conversions or YO/BaO (BaO/YO) interconversions in the ($a,b$) planes and extending over few nanometers along the $c$-axis. Structural models based on image matching with simulations are proposed for two particular cases. It is thought that these structural imperfections can be effective sites of flux pinning.

**Order No.: JA907-007** 

### Microstructures and solidification behavior in Y–Ba–Cu–O/Ag superconducting leads

J. Maeda, Y. Shiohara
*(ISTEC)*

The microstructures and the solidification behavior in unidirectionally solidified yttrium–barium–copper–oxide (YBCO)/Ag superconducting current leads were investigated. The solidification model of this system was discussed by the $Y_2Ba_1Cu_1O_5$–$Ba_3Cu_5O_x$–Ag quasiternary phase diagrams constructed by analysis of the solute compositions in the melt. The diffusion fields and the spacing between silver particles in the YBCO/Ag system were discussed. The relationship between the shapes of entrapped silver particulates, the miscibility gap in the phase diagram, and the wetting behavior at the growth interface in 2D monotectic reactions were also discussed.

**Order No.: JA907-008** 

### A model for the texture development of high-$T_c$ superconductors under an elevated magnetic field

P.J. Ferreira, H.B. Liu, J.B. Vander Sande
*(Massachusetts Institute of Technology)*

A theoretical model is proposed to explain the degree of texture achieved in high-$T_c$ superconductors during melt processing under an elevated magnetic field. The degree of grain alignment is quantified through a factor $F$ which is defined as ranging from 0 (random alignment) to 1 (completely oriented). Intermediate values of $F$ clearly characterize intermediate states of alignment where there is still some tendency for the grains to align their $c$-axis with the magnetic field. The model suggests that the enhancement in texture is primarily obtained through grain rotation during the early stages of grain growth from the liquid. At the later stages of growth, grains interact with each other, which hinders the phenomena of magnetic-field–induced grain alignment.

**Order No.: JA907-009** 

### Dislocation structure of low-angle grain boundaries in $YBa_2Cu_3O_{7-\delta}$/MgO films

S. Oktyabrsky[1], R. Kalyanaraman[2], K. Jagannadham[2], J. Narayan[2]
*([1]State University of New York—Albany, [2]North Carolina State University)*

Grain boundaries in laser-deposited $YBa_2Cu_3O_{7-\delta}$(YBCO)/MgO thin films have been investigated by high-resolution transmission electron microscopy. The films exhibit perfect texturing with YBCO(001)/MgO(001) giving rise to low-angle [001] tilt grain boundaries resulting from the grains with *c*-axis normal to the substrate surface with misorientation in the *a-b* plane. Atomic structure of the grain boundaries has been analyzed using a dislocation model. Low-angle grain boundaries have been found to be aligned along (100) and (110) interface planes. For (110) boundary plane, the low-energy dislocation configuration has been found to consist of an array of alternating [100] and [010] dislocations. We have calculated energy of various configurations and shown that the energy of the (110) boundary with dissociated dislocations is comparable to that of (100) boundary, which explains the coexistence of (100) and (110) interface facets along the boundary. We have also modeled critical current transport through grain boundaries with various structures and found that the low-energy (110) grain boundary with dissociated dislocation array is expected to transport lower superconducting current (by 25% for 6° misorientation) than (100) boundaries.

**Order No.: JA907-010** 

### X-ray and neutron diffraction of yttrium–barium–copper–oxide: Modeling diffraction intensity variations produced by surface leaching

S.A. Watkins, F.H. Cocks
*(Duke University)*

High normal current fluences have long been reported to produce major changes in the x-ray diffraction pattern of $YBa_2Cu_3O_{7-x}$ (YBCO). These x-ray diffraction effects have now been shown to result from the removal of barium from the YBCO near-surface lattice together with the formation of a thin barium oxide overlayer. Neutron diffraction reveals that the bulk crystallographic structure remains unaltered by charge fluences of more than 40 million C/cm$^2$, and Auger electron spectroscopy confirms the presence of surface barium enrichment.

**Order No.: JA907-011** 

### Structural, electrical, and optical property studies of indium-doped $Hg_{0.8}Cd_{0.2}Te/Cd_{0.96}Zn_{0.04}Te$ heterostructures

M.S. Han[1], T.W. Kang[1], T.W. Kim[2]
*([1]Dongguk University, [2]Kwangwoon University)*

Transmission electron microscopy (TEM), Hall effect, and Fourier transform infrared (FTIR) transmission measurements were performed to investigate the structural, electrical, and optical properties of indium-doped $Hg_{0.8}Cd_{0.2}Te$ epitaxial layers grown on $Cd_{0.96}Zn_{0.04}Te$ (211) B substrates by molecular-beam epitaxy. The TEM measurements showed that high-quality $Hg_{0.8}Cd_{0.2}Te$ epitaxial layers with interfacial abruptnesses were grown on the $Cd_{0.96}Zn_{0.04}Te$ substrates. The Van der Pauw Hall effect measurements on typical indium-doped $Hg_{0.8}Cd_{0.2}Te/Cd_{0.96}Zn_{0.04}Te$ heterostructures with a doping concentration of $6 \times 10^{16}$ cm$^{-3}$ at 10 K in a magnetic field of 0.5 T yielded a carrier density and a mobility of $2.2 \times 10^{16}$ and cm$^{-3}$ and 4000 cm$^2$/V s, respectively. The FTIR spectra showed that the absorption edges of the indium-doped $Hg_{0.8}Cd_{0.2}Te/Cd_{0.96}Zn_{0.04}Te$ heterostructures shifted to the shorter wavelength range in comparison to those of the undoped samples, which was caused by the Burstein–Moss effect. The FTIR spectra also showed that the transmittance intensities of the indium-doped $Hg_{0.8}Cd_{0.2}Te/Cd_{0.96}Zn_{0.04}Te$ heterostructures increased in comparison to those of the undoped heterostructures; this is due to the compensation of the Hg vacancy defects by the indium atoms. These results indicate that the indium-doped $Hg_{0.8}Cd_{0.2}Te$ epitaxial layers were high-quality n-type layers and that p-$Hg_xCd_{1-x}Te$ epilayers can be grown on indium-doped $Hg_{0.8}Cd_{0.2}Te/Cd_{0.96}Zn_{0.04}Te$ heterostructures for the fabrication of $Hg_xCd_{1-x}Te$ photoconductors and photodiodes.

**Order No.: JA907-012** 

### On temperature dependence of deformation mechanism and the brittle–ductile transition in semiconductors

P. Pirouz[1], A.V. Samant[1], M.H. Hong[1], A. Moulin[2], L.P. Kubin[2]
*([1]Case Western Reserve University, [2]CNRS-ONERA)*

Recent deformation experiments on semiconductors have shown the occurrence of a break in the variation of the critical resolved shear stress of the crystal as a function of temperature. These and many other examples in the literature evidence a critical temperature at which a transition occurs in the deformation mechanism of the crystal. In this paper, the occurrence of a similar transition in two polytypes of SiC is reported and correlated to the microstructure of the deformed crystals investigated by transmission electron microscopy, which shows evidence for partial dislocations carrying the deformation at high stresses and low temperatures. Based on these results and data in the literature, the explanation is generalized to other semiconductors and a possible relationship to the brittle–ductile transition is proposed.

**Order No.: JA907-013** 

### Photovoltaic spectroscopic study of GaN epilayers and InGaN quantum well structures

W. Liu[1], M.F. Li[1], K.L. Teo[1], N. Akutsu[2], K. Matsumoto[2]
*([1]The National University of Singapore, [2]Nippon Sanso Co.)*

Room-temperature photovoltaic spectroscopy was applied to study undoped GaN, n-type GaN, and InGaN quantum well structures. Clear exciton absorption was observed in the photovoltaic spectra of the undoped GaN, and polarization measurements were made to identify the exciton absorption. For the n-type GaN sample, instead of the exciton absorption we observed only bulk absorption edge, which may have been due to the free carrier screening effect. For the InGaN quantum well structures, the photovoltaic spectra showed relatively complicated line shape due to the overlap of the signals from different layers. By changing the reference phase of the lock-in amplifier, we were able to suppress some of the signals and thus identify the origin of the corresponding signal.

**Order No.: JA907-014** 

### Ordered γ-brass structures coexisting with the decagonal quasicrystal in a $Ga_{46}Fe_{23}Cu_{23}Si_8$ alloy

S.P. Ge, K.H. Kuo
*(Chinese Academy of Sciences)*

In a moderately rapidly solidified $Ga_{46}Fe_{23}Cu_{23}Si_8$ alloy, a fcc superstructure with $a = 1.78$ nm and a hexagonal superstructure with $a_{hex} = 2.18$ nm and $c_{hex} = 0.77$ nm, based on the same bcc γ-brass structure with $a = 0.89$ nm, were found—by means of micro-area diffraction—to coexist with the decagonal quasicrystal. The fcc superstructure is probably similar to one of the F-centered γ-brass structure and has a parallel orientation relationship with the bcc fundamental structure. The hexagonal superstructure has its (001) parallel to the $(11\bar{1})$ of the bcc γ-brass structure and its $c_{hex} = a_{bcc}[11\bar{1}]/2$, and their lattice correspondence relationship has been derived. Electron diffraction evidence is presented to show that these two superstructures are possibly crystalline approximants of the decagonal quasicrystal.

**Order No.: JA907-015** 

### Evolution of martensitic transformation in Cu–Al–Ni shape memory alloys during low-temperature aging

V. Recarte, R.B. Pérez-Sáez, M.L. Nó, J. San Juan
*(Universidad del País Vasco)*

The effect of thermal aging at 473 K on martensitic transformation characteristics has been studied in the Cu–Al–Ni shape memory alloys. An increase of martensitic transformation temperatures as a result of aging has been observed. Furthermore, the martensitic transformation shows an evolution with aging time from a single $\beta_3 \Rightarrow \gamma'_3 + \beta'_3$ transformation. Using internal friction and thermoelectric power measurements, as well as specific thermal treatments, it has been determined that the mechanism responsible for this evolution is an increase in the degree of order, thus rejecting the participation of a $\gamma_1$ precipitation process. Finally, the increase of order at the next nearest neighbors has been established as the main factor responsible for the evolution of the martensitic transformation characteristics.

**Order No.: JA907-016** 

### Effect of secondary phase particles on post-recrystallization grain growth in reactive spray deposited 5083 Al alloys

S.L. Dai[1], J-P. Delplanque[2], E.J. Lavernia[3]
*([1]Beijing Institute of Aeronautical Materials, [2]Colorado School of Mines, [3]University of California—Irvine)*

Grain growth behavior in reactive spray deposited Al–Mg–Mn alloy 5083 and 5083 + Zr was quantitatively studied at 500, 530, and 560 °C. Results showed that reactive spray deposited 5083 processed using $N_2$–5% $O_2$, in which no significant volume fraction of oxide particles was found, experienced significant grain growth when annealed at 500, 530, and 560 °C following recrystallization. On the other hand, reactive spray deposited 5083 atomized

with $N_2$–10% $O_2$ and 5083 + Zr atomized with $N_2$–5% $O_2$ exhibited very slow grain growth below 530 °C and limited grain growth at 560 °C. This behavior was attributed to the retardation effect of the secondary phase particles that were formed in these alloys.
**Order No.: JA907-017** 

### Phase stability of Ni–Al nanoparticles

S. Ramos de Debiaggi[1], J.M. Campillo[2], A. Caro[3]
*([1]Universidad Nacional del Comahue, [2]Euskal Herriko Unibertsitatea, [3]Centro Atómico Bariloche)*

The phase stability of Ni–Al clusters of nanometer size was studied using the embedded atom model and Monte Carlo simulation techniques. For temperatures of 500 and 1000 K and for a range of compositions below 70 at.% Al, the equilibrium structures of the system were determined and compared to the bulk results. We found that the bulk NiAl (B2) and $Ni_3Al$ ($L1_2$) phases were stable phases in the nanoparticle system; however, for deviations from ideal composition, the analysis revealed that due to the surface effect, the composition of the clusters was not uniform. There was a core region in which the structure was ordered, B2 or $L1_2$, with composition very close to the ideal, and a chemically disordered mantle region that allocated the deviations from ideal stoichiometries; in this way, larger phase field appeared, indicating similar trends as found in experiments on nanocrystalline Ni–Al powder [S.K. Pabi and B.S. Murty, Mater. Sci. Eng., **A214** 146 (1996)]. For concentrations between 37 and 51 at.% Al, an intermediate phase, similar to the tetragonal $L1_0$ martensite, appeared.
**Order No.: JA907-018** 

### First principles study of influence of alloying elements on TiAl: Lattice distortion

Y. Song[1], R. Yang[1], D. Li[1], W.T. Wu[1], Z.X. Guo[2]
*([1]Chinese Academy of Sciences, [2]University of London)*

The influences of ternary additions of Cr, Fe, Mn, Ni, Zr, Nb, Mo, Hf, Ta, Si, Ga, Ge, In, and Sb, as well as the anti-site defects of both Ti and Al on lattice parameters of TiAl, were studied by the first principles electronic structure calculations with a discrete variational cluster method. The results of calculation showed that the effect of ternary additions on the distortion of TiAl lattice varied with the substitution behavior of the individual alloying element involved. The addition of alloying elements in TiAl caused a change in the electronic structure and the density of states of the system and resulted in variation of the bond strength between the atoms. The total partial density of states (DOS) of binary TiAl and of ternary TiAl–*M*, *M* = Cr, Zr, and Sb etc. were comparatively examined. The relationship between the DOS and the bond strength was discussed. The present work suggests that the origin of the lattice distortion of the ternary TiAl–*M* systems lies in the variation of the electronic structure.
**Order No.: JA907-019** 

### Dependence of the mechanical and structural properties of (Ti,Al)N films on the nitrogen content

C. Jiménez[1], C. Sánchez-Fernández[1], C. Morant[1], J. Sánchez-Olías[2], J.M. Martínez-Duart[1], M. Fernández[2]
*([1]Universidad Autónoma de Madrid, [2]C.S.I.C.)*

(Ti,Al)N films with increasing nitrogen content were grown by reactive cosputtering and characterized by auger electron spectroscopy, grazing x-ray diffraction, polarization curves, electrochemical impedance spectroscopy, nanoindentation, and atomic force microscopy. For Ti/Al ≈ 1 the $Ti_{1-x}Al_xN$ phase is always present, but lower nitrogen contents lead to an additional phase, probably α–Ti(Al), which causes a decrease in hardness and Young's modulus. According to the impedance results, the increase of nitrogen content results in a decrease of surface roughness or a more compacted surface coating.
**Order No.: JA907-020** 

### High-strain-rate response of hot-explosively consolidated W–Ti alloys

L.J. Kecskes[1], I.W. Hall[2]
*([1]U.S. Army Research Laboratory, [2]University of Delaware)*

Disk-shaped, two-phase, full-density W–Ti alloy billets have been fabricated by a new, hot-explosive-compaction technique. As part of a characterization effort, the compressive behavior of the alloy was investigated. Quasistatic and split Hopkinson pressure bar (SHPB) tests of cylindrical samples, taken from a 83W–17 Ti at.% alloy billet, demonstrate the propensity of this material to fail via shear localization at high strain rates. The effects of strain rate, orientation of the matrix phase with respect to the direction of the SHPB compression, and spatial location within the billet (i.e., periphery or core) were evaluated. At quasistatic strain rates, the alloy deformed in a ductile mode and exhibited a definite spatial location sensitivity. At high strain rates, spatial location sensitivity was absent. Shear localization was unaffected by density variations, matrix orientation in the alloy, or the presence of coarsened substructural features in the matrix. These experiments and the microstructural characteristics of the resultant localized regions are discussed.
**Order No.: JA907-021** 

### Synthesis of magnetic particle/organic hybrid from metalorganic compounds

T. Yogo, T. Nakamura, W. Sakamoto, S. Hirano
*(Nagoya University)*

A nanocrystalline magnetic particle/oligomer hybrid was successfully synthesized by polymerization of iron(III)3-allylacetylacetonate (IAA) followed by *in situ* hydrolysis. An iron oxide particle/oligomer hybrid was synthesized by hydrolysis of the IAA oligomer under alkaline and reducing condition by addition of hydrazine or methylhydrazine. Crystalline particles of about 10 nm in size were found to be dispersed in the oligomeric matrix. The nanocrystalline particles were identified to be iron oxide spinel by x-ray diffraction analysis and electron diffraction. The nanometer-sized ferrimagnetic iron oxide particle/oligomer hybrid showed a typical superparamagnetic behavior.
**Order No.: JA907-022** 

### Magnetization of carbon-coated ferromagnetic nanoclusters determined by electron holography

S. Seraphin[1], C. Beel[2], J-M. Bonard[2], J. Jiao[1], P.A. Stadelmann[2], A. Châtelain[2]
*([1]University of Arizona, [2]Ecole Polytechnique Fédérale de Lausanne)*

The magnetic properties of carbon-coated Co and Ni nanoparticles aligned in chains were determined using transmission electron holography. The measurements of the phase change of the electron wave due to the magnetization of the sample were performed. The ratio of remnant magnetization to bulk saturation magnetization $M_r/M_s$ of Co decreased from 53% to 16% and of Ni decreased from 70% to 30% as the particle diameter increased from 25 to 90 nm. It was evident that the inhomogenous magnetic configurations could diminish the stray field of the particles. After being exposed to a 2-Tesla external magnetic field, the $M_r/M_s$ of Co increased by 45% from the original values with the same dependency on the particle size. The $M_r/M_s$ of Ni particles, on the other hand, increased only 10%. The increased magnetization could be attributed to the merging of small domains into larger ones after the exposure to the external magnetic field. The validity of the interpretation of the holograms was established by simulation.
**Order No.: JA907-023** 

### Mechanical properties of vapor-grown carbon fiber composites with thermoplastic matrices

G.G. Tibbetts, J.J. McHugh
*(General Motors R & D Center)*

This paper discusses the mechanical properties of vapor-grown carbon fiber (VGCF)/nylon and VGCF/polypropylene composites. Fibers in the as-produced condition yielded composites with marginally improved mechanical properties. Microscopic examination of these composites clearly showed regions of uninfiltrated fibers, which could account for the unsatisfactory mechanical properties. The infiltration of the fibers by both polymers was improved by carefully ball milling the raw fiber so as to reduce the diameter of the fiber clumps to less than 300 μm. Properties of composites made with ball-milled material were improved in every respect. VGCF reinforcement in nylon slightly improved the tensile strength and doubled the modulus, while VGCF in polypropylene doubled the tensile strength and quadrupled the modulus compared to unreinforced material. Moreover, the composites were sufficiently improved that differences in fiber surface preparation became important. For example, air-etched fibers and fibers covered with low concentrations of aromatics produced polypropylene composites with significantly better mechanical properties than did fibers whose surfaces were heavily coated with aromatics. Both the tensile strength and the modulus of the composites fabricated with clean fibers exceeded theoretical values for composites made with fibers randomly oriented in 3 dimensions, indicating that the injection molding process oriented the fibers to some extent.
**Order No.: JA907-024** 

### Assessment of single-fiber fragmentation using scanning acoustic microscopy

S. Sathish[1], M.S. Madhukar[2], J.H. Cantrell[3], W.T. Yost[3]
*([1]University of Dayton, [2]University of Tennessee, [3]NASA Langley Research Center)*

Scanning acoustic microscopy (SAM) was used to obtain the critical fragmentation length of 7-μm-diameter carbon fiber embedded in an optically transparent epoxy matrix and subjected to a standard fiber fragmentation test. The SAM-assessed critical fragmentation length of (356 ± 59.5) μm compared favorably with the value (341 ± 52.3) μm obtained independently from commonly used photoelastic techniques. Additionally, the SAM images allowed an assessment of regions of fiber-matrix debond, including the measurement of an average debond of (61.0 ± 11.8) μm along the fiber from the fragment ends, which could not be obtained with photoelastic methods. The application of SAM to the assessment of optically opaque composite materials is explained in this paper.

**Order No.: JA907-025** 

### Investigation of interfacial phenomena in Ag/Si multilayers during the annealing process

J.H. Zhao[1,2], M. Zhang[1], R.P. Liu[1], X.Y. Zhang[1], L.M. Cao[1], D.Y. Dai[1], H. Chen[1], Y.F. Xu[1], W.K. Wang[1,2]
*([1]Chinese Academy of Sciences, [2]Yanshan University)*

Interfacial phenomena and microstructure in Ag/Si multilayers with a modulation period of 7.64 nm during annealing from 323 to 573 K were investigated by *in situ* x-ray diffraction and high-resolution transmission electron microscopy. Uphill and downhill diffusion were observed on annealing. The temperature dependence of the effective diffusion coefficient from 373 K (as to downhill diffusion regime) to 523 K was $D_e = 2.02 \times 10^{-20} \exp(-0.24\ eV/k_BT)\ m^2/s$. Diffusion of silicon atoms along silver grain boundaries was proposed as the main diffusion mechanism. After annealing, continuous silver sublayers changed to nanometer-sized silver particles (about 4.5 nm) coated completely by amorphous silicon.

**Order No.: JA907-026** 

### Polymer-bonded magnets: Part I. Analytic thermogravimetry to determine the effect of surface modification on dispersion of Nd–Fe–B fillers

J. Xiao, J.U. Otaigbe
*(Iowa State University of Science and Technology)*

The degree of mixing is a critical factor in controlling the magnetic properties and mechanical properties of polymer-bonded magnets. Pretreatment of the NdFeB fillers with a silane coupling agent improved the degree of mixing of the fillers in the polymer matrix. The observed improvement in the degree of mixing of the silane-treated fillers was ascribed to good wetting as evidenced by viscosity reduction of the coupled polymer-bonded magnets. However, traditional materials characterization methods could not be used to quantitatively determine the degree of mixing of the polymer-bonded magnets. This paper describes use of thermogravimetric analysis (TGA) to quantify the degree of mixing of polymer-bonded magnets. The intensity of segregation of the fillers was calculated from the measured weight change of the magnetic filler in the samples. The results of this work showed that the TGA method was useful in determining the degree of mixing of NdFeB fillers in polymer-bonded magnets.

**Order No.: JA907-027** 

### Synthesis of surface metallized polymeric films via *in situ* reduction of (4,4,4-trifluoro-1-(2-thienyl)-1,3-butanedionato)silver(I) in a polyimide matrix

R.E. Southward[1], C.K. Bagdassarian[2], C.J. Sudol[2], J.L. Wasyk[2], S.H. Sproul[2], S.T. Broadwater[2], J.L. Scott[2], D.W. Thompson[2]
*([1]NASA-Langley Research Center, [2]College of William and Mary)*

Thermal curing of the (4,4,4-trifluoro-1-(2-thienyl)-1,3-butanedionato)silver(I)-containing poly(amic acid) formed from 3,3′,4,4′-benzophenone tetracarboxylic acid dianhydride (BTDA) and 4,4′-oxydianiline (4,4′-ODA) in dimethylacetamide gave both polyimide films via cyclodehydration and reduction of silver(I) to the native metal. Silver(0) migrated to the surface resulting in surface metallized composite films, which could have excellent reflectivity but did not exhibit surface electrical conductivity. The films retained mechanical and thermal properties similar to those of the parent polyimide. X-ray diffraction showed crystalline face-centered-cubic silver in the films after thermal curing. Microscopy data showed that the surfaces particle sizes were in the range of approximately 50–100 nm. Significant silver remained in the bulk of the polyimide film with varying particles sizes generally less than approximately 15 nm. The interior of the metallized films was not electrically conducting. Films were characterized by x-ray diffraction, differential scanning calorimetry, thermal gravimetric analysis, x-ray photoelectron spectroscopy, transmission electron microscopy, scanning electron microscopy, and mechanical measurements.

**Order No.: JA907-028** 

### Structural characterization of laser-ablated epitaxial $(Ba_{0.5}Sr_{0.5})TiO_3$ thin films on MgO(001) by synchrotron x-ray scattering

S. Kim[1], T.S. Kang[2], J.H. Je[2]
*([1]Sunchon National University, [2]Pohang University of Science and Technology)*

Epitaxial $(Ba_{0.5}Sr_{0.5})TiO_3$ thin films of two different thickness (~25 nm and ~134 nm) on MgO(001) prepared by a pulsed laser deposition method were studied by synchrotron x-ray scattering measurements. The film grew initially with a cube-on-cube relationship, maintaining it during further growth. As the film grew, the surface of the film became significantly rougher, but the interface between the film and the substrate did not. In the early stage of growth, the film was highly strained in a tetragonal structure ($c/a = 1.04$) with the longer axis parallel to the surface normal direction. As the growth proceeded further, it relaxed to a cubic structure with the lattice parameter near the bulk value, and the mosaic distribution improved significantly in both in- and out-of-plane directions. The thinner film (~25 nm) showed only one domain limited mainly by the film thickness, but the thicker film (~134 nm) exhibited three domains along the surface normal direction.

**Order No.: JA907-029** 

### Growth of graphite nanofibers from the decomposition of $CO/H_2$ over silica-supported iron–nickel particles

P.E. Anderson, N.M. Rodriguez
*(Northeastern University)*

Extremely fine, tubular graphite nanofibers of varying geometries and degrees of crystallinity were produced by the decomposition of CO and hydrogen over various compositions of nickel–iron particles supported on silica. High-resolution transmission electron microscopy coupled with temperature programmed oxidation studies revealed that as the iron content of the catalyst was increased, the bimetallic particles precipitated a chainlike graphitic fibrous structure in a stepwise mechanism. The high-iron-content system Fe–Ni (8 : 2) yielded a small amount of these chainlike graphite fibers that were extremely resilient to oxidation, suggesting a highly crystalline structure. When the catalyst particles consisted of a nickel–iron mixture Fe–Ni (5 : 5) there was a decrease in the degree of crystallinity of the fibers (78% graphite) and a corresponding increase in the amount of amorphous carbon precipitated (22% amorphous) within the structure. The high-nickel catalyst Fe–Ni (2 : 8) generated the largest amount of the tubular nanofiber product. It was significant that there was an increase in the amorphous carbon content (58%) precipitated as opposed to graphitic carbon (42%) in the structures. In some cases, amorphous carbon was deposited inside the graphite core of the nanofibers. The influence of the catalyst composition and nature of the metal-support interaction are key factors in the continuing development of graphite nanofibers possessing desired structures for potential uses in a variety of applications.

**Order No.: JA907-030** 

### Kinetics and mechanism of anatase-to-rutile phase transformation in the presence of borosilicate glass

J-H. Jean, S-C. Lin
*(National Tsing Hua University)*

The effects of borosilicate glass (BSG) on the kinetics and mechanism of anatase-to-rutile phase transformation have been investigated. The displacive anatase-to-rutile phase transformation kinetics of $TiO_2$ were greatly enhanced in the presence of BSG. The transformation kinetics followed Avrami equation, and the results showed an apparent activation energy of 260–370 kJ/mol, which was close to the bond strength of Ti–O, suggesting a reaction-controlling mechanism. The values of the Avrami exponent were in the range of 1.4–2.3, which could be interpreted as 2-dimensional reaction-controlled growth at zero nucleation rate. The rutile particles obtained by the phase transformation were always much larger than the starting anatase powders, which was explained by a mechanism of phase-transformation–induced particle coalescence.

**Order No.: JA907-031** 

### Equilibrium phases in Mn–V–O system under ambient atmosphere

S.K. Chung[1], A.A. Andriiko[2], P.V. Rudenok[2], S.J. Shin[1]
*([1]World-Peace Institute of Technology, [2]Institute of General and Inorganic Chemistry)*

The products obtained from $MnO_2$–$V_2O_5$ mixtures at the ambient oxygen pressure and temperatures up to 900 °C were studied by means of thermal analysis and x-ray diffraction methods. The following phases were found to exist in equilibrium, depending on the composition: I. $Mn_2O_3$–$Mn_2V_2O_7$, II. $Mn_2V_2O_7$–$MnV_2O_6$, and III. $V_2O_5$-solid solution of $VO_2$ in $MnV_2O_6$. A phase diagram was obtained for the composition region III. The data were instructive for syntheses of manganese vanadates by thermal methods.

**Order No.: JA907-032** 

### Solution deposition processing and electrical properties of $Ba(Ti_{1-x}Sn_x)O_3$ thin films

K.H. Yoon, J.H. Park, J.H. Jang
*(Yonsei University)*

$Ba(Ti_{1-x}Sn_x)O_3$ ($0 \leq x \leq 0.3$) thin films were deposited on a platinized silicon substrate by a solution deposition process utilizing methoxyethanol, water, and propylene glycol as solvents. Dielectric properties and current-voltage characteristics of the thin films were investigated in conjunction with phase evolution and microstructures by varying heating temperatures and Sn contents ($x$). Thin films annealed above 700 °C showed a pure perovskite phase with nanoscaled grains (20–30 nm). The dielectric constant of the thin films depended on the Sn content and showed a maximum value of 330 at $x$ = 0.15. The leakage current behavior of an optimum composition corresponding to $x$ = 0.15 was examined by correlating with charge transport mechanisms. Schottky emission was found to be predominant at voltages less than 6.8 V, while Fowler–Nordheim tunneling appeared to be responsible above 6.8 V. The Schottky barrier of the $Ba(Ti_{0.85}Sn_{0.15})O_3$/Pt interface was determined to be 1.49 eV.

**Order No.: JA907-033** 

### Crack tip 90° domain switching in tetragonal lanthanum-modified lead zirconate titanate under an electric field

F. Fang, W. Yang, T. Zhu
*(Tsinghua University)*

Lanthanum-modified lead zirconate titanate ferroelectric ceramics $(Pb_{0.96}La_{0.04})(Zr_{0.40}Ti_{0.60})_{0.99}O_3$ were synthesized by the conventional powder processing technique. X-ray diffraction experiments revealed that the samples belong to the tetragonal phase with $a = b = 0.4055$ nm, $c = 0.4109$ nm, and $c/a = 1.013$. After being poled, the samples were indented by a 5-kg Vickers indenter, and lateral electric fields of 0.4 $E_c$, 0.5 $E_c$, and 0.6 $E_c$ ($E_c$ = 1100 V/mm) were applied, respectively. Field emission scanning electron microscopy showed that 90° domain switching appeared near the tip of the indentation crack under a lateral electric field of 0.6 $E_c$. A mechanism of 90° domain switching near the crack tip under electric field is discussed.

**Order No.: JA907-034** 

### Thermally induced structural changes in epitaxial $SrZrO_3$ films on $SrTiO_3$

P.A. Langjahr[1], T. Wagner[1], M. Rühle[1], F.F. Lange[2]
*([1]Max-Planck-Institut für Metallforschung, [2]University of California)*

Epitaxial, continuous, approximately 40-nm-thick films of $SrZrO_3$ on $SrTiO_3$ substrates prepared by a chemical solution deposition method including a post-deposition heat treatment at 900–1000 °C were subjected to further heat treatments at higher temperatures (approximately 1200–1300 °C) to investigate their high temperature stability. Experimental investigations included scanning electron microscopy, atomic force microscopy, and conventional transmission electron microscopy. The investigations have demonstrated a morphological instability of the films. Concentration profiles of the cations determined by energy dispersive x-ray spectroscopy, as well as investigations by x-ray diffraction revealed that the film islands consisted of a solid solution. As shown by high-resolution electron microscopy, the reaction between film and substrate also led to an increase in the separation distance of the misfit dislocations that were introduced during the lower temperature heat treatment to relax the lattice mismatch strain. The morphological and structural changes of the films are reported and discussed in this paper.

**Order No.: JA907-035** 

### Nucleation mechanisms in chemically vapor deposited mullite coatings on SiC

P. Hou, S.N. Basu, V.K. Sarin
*(Boston University)*

Dense, uniform, and adherent chemically vapor deposited mullite coatings were deposited on SiC substrates using the $AlCl_3$–$SiCl_4$–$H_2$–$CO_2$ system. Typical coating morphology consisted of a thin interfacial layer of $\gamma$–$Al_2O_3$ nanocrystallites imbedded within a vitreous $SiO_2$-based matrix. When a critical Al/Si ratio of 3.2 ± 0.29 was reached within this nanocrystalline layer, mullite crystals nucleated and grew as columnar grains. The thickness of the nanocrystalline layer decreased as the input $AlCl_3/SiCl_4$ ratio was increased. In all cases, the Al/Si composition in the coating increased from the coating/substrate interface to the coating surface. Critical factors leading to the nucleation and growth of mullite crystals are discussed in this paper.

**Order No.: JA907-036** 

### Transmission electron microscopy observation of second-phase particles in $\beta$–$Si_3N_4$ grains

N. Hirosaki[1], T. Saito[2], F. Munakata[3], Y. Akimune[3], Y. Ikuhara[4]
*([1]National Institute for Research in Inorganic Materials, [2]Japan Fine Ceramic Center, [3]Nissan Motor Co., Ltd., [4]The University of Tokyo)*

Silicon nitride was fabricated by adding $Y_2O_3$ and $Nd_2O_3$ as sintering additives, sintering for 8 h at 1900 °C, and heat treating for 4 h at 2200 °C to enhance grain growth. The microstructure was investigated by scanning electron microscopy, high-resolution electron microscopy, energy dispersive x-ray spectroscopy (EDS), and electron microdiffraction. This material had a duplex microstructure composed of many fine grains and a small number of coarse grains. In $\beta$–$Si_3N_4$ grains, second-phase particles with the composition of liquid phase, Y–Nd–Si–O or Y–Nd–Si–O–N, in the size of 10–30 nm were observed. EDS spectra and microdiffraction patterns revealed that those were amorphous or crystalline particles of Y–Nd-apatite, $(Y,Nd)_{10}Si_6O_{24}N_2$. These particles were presumably formed during cooling by the precipitation of Y–Nd–Si–O–N, which was trapped in the $\beta$–$Si_3N_4$ grains as solid solution or trapped liquid. The results suggest that attention should be paid to the trace amounts of trapped elements in $\beta$–$Si_3N_4$ grains in trying to improve the thermal conductivity of sintered silicon nitride.

**Order No.: JA907-037** 

### Microstructure in silicon nitride containing $\beta$-phase seeding

H-H. Lu, J-L. Huang
*(National Cheng-Kung University)*

A proper powder preparation technique was used to develop elongated $\beta$–$Si_3N_4$ particles as seeds from raw materials. The phase transformation and development of microstructure in $Si_3N_4$ ceramics containing $\beta$–$Si_3N_4$ seeds were investigated. The specimens of seeded silicon nitride had higher phase transformation rates than the specimens without seed. A core/shell structure was observed by transmission electron microscopy in seeded specimens owing to the difference in aluminum concentration in $Si_3N_4$ grains. The misfit between the core and the shell was accommodated by interfacial dislocation that had a rotation character. The growth mode was epitaxial, although there was some compositional difference between the core and the shell. A relatively larger grain size and wider grain size distribution in seeded $Si_3N_4$ specimens was due to the amount of $\beta$-phase seeds that could act as the nuclei, and the final modification of the microstructure was due to the coalescence process. The crack wake process characterized the mechanism of toughening.

**Order No.: JA907-038** 

### Origin of strength change in ceramics associated with the alteration of spray dryer

T. Hotta[1], K. Nakahira[1], M. Naito[1], N. Shinohara[2], M. Okumiya[2], K. Uematsu[3]
*([1]Japan Fine Ceramics Center, [2]Asahi Grass Co., [3]Nagaoka University)*

A significant difference of strength was noted in alumina ceramics made through the powder compaction process with spray dryers of two sizes. The origin of the change was examined with new characterization methods involving optical microscopy. The granules were found to have irregular shape. Defects in compacts were formed from these dimples and also from the nonuniform packing of powder particles at the granule boundaries. These defects are responsible for major defects in sintered bodies. The change of strength in the ceramics can be explained by the change of granule size with the spray dryer. The size of granules was found to directly affect the size of defects in the green and sintered bodies. The size of granules, defects in granules, green bodies and sintered bodies were approximately 20–30% smaller for granules made with the small spray dryer. There was a direct correlation between the size of defect and the strength of ceramics.

**Order No.: JA907-039** 

### Formation and characterization of hydroxyapatite coating layer on Ti-based metal implant by electron-beam deposition

J-M. Choi[1], Y-M. Kong[1], S. Kim[1], H-E. Kim[1], C.S. Hwang[1], I-S. Lee[2]
*([1]Seoul National University, [2]Research Center of Orthopaedic & Rehabilitation Engineering)*

A hydroxyapatite [HAp; $Ca_{10}(PO_4)_6(OH)_2$] coating layer was formed on a Ti-based alloy by the electron-beam deposition method. When pure HAp was used as a target for the deposition, an amorphous layer was formed on the metal substrate. By heat treatment in a vacuum at 630 °C, the layer was crystallized into tricalcium phosphate [TCP; $Ca_3(PO_4)_2$]. The crystallization improved the dissolution rate of the layer remarkably; however, at the same time, it deteriorated the bond strength with the substrate. When extra CaO (up to 25 wt%) was added to the target and processed under the same conditions, a layer compositionally close to crystalline HAp was deposited. Before the heat treatment, even though the layer was in amorphous state, the dissolution rate in the physiological solution was extremely low. Furthermore, the bond strength increased remarkably compared to the layer formed by the pure HAp target. Compositional and structural resemblance of the layer with the crystalline HAp was attributed to these improvements in properties.

**Order No.: JA907-040** 

### Bismuth composition control of $SrBi_2TaNbO_9$ thin films by heat treating $Bi_2O_3$-inserted heterostructure

Y-B. Park[1], J-K. Lee[1], H-J. Jung[1], J-W. Park[2]
*([1]Korea Institute of Science and Technology, [2]Hanyang University)*

Ferroelectric properties of $SrBi_2TaNbO_9$ (SBTN) thin films were changed by the amount of Bi content in SBTN. We proposed that the addition of excess Bi into the SBTN thin films could be accomplished by heat treating the SBTN/$Bi_2O_3$/SBTN heterostructure fabricated by the rf magnetron sputtering method. The Bi composition was controlled by changing the thickness of the inserted $Bi_2O_3$ from 50 to 400 Å in the SBTN/$Bi_2O_3$/SBTN heterostructure. As the thickness of $Bi_2O_3$ films was increased from 0 to 100 Å, the grain grew faster and the ferroelectric properties improved. On the other hand, when the thickness of $Bi_2O_3$ films was thicker than 150 Å, the ferroelectric properties deteriorated. In particular, when a 400-Å $Bi_2O_3$ layer was inserted between SBTN films, a $Bi_2Pt$ phase appeared, and the $Bi_2O_3$ films remained between SBTN films, resulting in poor ferroelectric properties. A $Bi_2Pt$ phase was formed by the reaction between the platinum bottom electrode and $Bi_2O_3$ films. On the other hand, the leakage current density of SBTN thin films decreased with the increase of inserted $Bi_2O_3$ film thickness. As the thickness of inserted $Bi_2O_3$ films was increased from 0 to 50 Å, leakage current density abruptly decreased because Bi content of the SBTN thin films was increased from 8 mol% deficient to stoichiometric composition. As the thickness of inserted $Bi_2O_3$ films increased from 100 to 400 Å, leakage current density gradually decreased because the remaining $Bi_2O_3$ layer in SBTN thin films increased.

**Order No.: JA907-041** 

### Design for high-performance functional composite thermistor materials by glass/ceramic composing

D.J. Wang, J. Qiu, Z.L. Gui, L.T. Li
*(Tsinghua University)*

A NTC-PTC composite thermistor with high-performance was designed by glass/ceramic composing. The material exhibited low resistivity and a large negative temperature coefficient of resistivity. The minimum resistivity was at the magnitude of $10^2$ Ω cm, and the negative temperature coefficient of resistivity was better than –3% $°C^{-1}$. The results showed that the large negative temperature coefficient of resistivity was closely related to the glass phase, and the NTC-PTC functional composite material was a kind of grain-boundary-controlled material.

**Order No.: JA907-042** 

### The morphology and growth mechanism of alumina whiskers in aluminum-based metal matrix composites

Y-F. Li, C-D. Qin, D.H.L. Ng
*(The Chinese University of Hong Kong)*

A process has been invented for growing alumina ($Al_2O_3$) whiskers in the matrix of the aluminum-based metal matrix composite by the internal oxidation reaction between aluminum (Al) and molybdenum oxide ($MoO_3$) at 850 °C. The whiskers were formed during the firing stage and distributed uniformly throughout the metal matrix. The fractional volume of the whiskers was about 30%, and their average size was 1 μm in diameter and 10 μm in length. The growth mechanism of the $Al_2O_3$ whiskers was studied. It was found that the nutrient for the growth of the whiskers was supplied from the molten Al at the base of the whiskers where they reacted with $MoO_3$ forming the $Al_2O_3$ whiskers and the Al–Mo intermetallic phases.

**Order No.: JA907-043** 

### Powder synthesis of barium titanate and barium orthotitanate via an ethylene glycol complex polymerization route

S.J. Lee, M.D. Biegalski, W.M. Kriven
*(University of Illinois—Urbana-Champaign)*

Pure and reactive barium titanate ($BaTiO_3$) and barium orthotitanate ($Ba_2TiO_4$) powders have been synthesized by an ethylene glycol, polymerization-complexation route. The ethylene glycol content affected the crystallization behavior and powder morphology. The $BaTiO_3$ powder, which had a particle size of 100 nm, crystallized from amorphous to tetragonal phase on calcining at 700 °C for 1 h. Ball-milled $BaTiO_3$ powder sintered to 97% relative density at 1200 °C after 2 h, with a grain size of approximately 200 nm. $Ba_2TiO_4$ powder required longer holding times or higher temperatures to be crystallized from the amorphous phase than did $BaTiO_3$. In $Ba_2TiO_4$, the phase transformation between low-temperature monoclinic symmetry to high-temperature orthorhombic symmetry was observed by dilatometry and differential scanning calorimetry. A volume decrease of approximately 0.5% accompanied the monoclinic to orthorhombic transformation on heating. The high-temperature orthorhombic phase could be retained down to room temperature by the addition of at least 6 wt% magnesia (MgO) stabilizer.

**Order No.: JA907-044** 

### Quantitative adhesion measures of multilayer films: Part I. Indentation mechanics

M.D. Kriese[1], N.R. Moody[2], W.W. Gerberich[1]
*([1]University of Minnesota, [2]Sandia National Laboratories)*

The mechanics for calculating the quantitative driving force of indentation-induced delamination of thin film multilayers is presented. The solution is based on the mechanics developed by Marshall and Evans [D.B. Marshall and A.G. Evans, J. Appl. Phys. **56**, 2632–2638 (1984)] and extended to the general case of a multilayer by use of standard bending and thin plate analyses. Specific solutions for the bilayer case are presented and discussed, which show that in the limit of zero thickness of either layer, the solution converges to the single-layer case. In the range of finite thickness, the presence of the superlayer increases the driving force relative to that possible for the original film alone and can be optimized to the experimental situation by proper choice of thickness, elastic constants, and residual stress. The companion paper "Quantitative adhesion measures of multilayer films: Part II. Indentation of W/Cu, W/W, Cr/W" discusses experimental results with copper, tungsten, and chromium thin films.

**Order No.: JA907-045** 

### Quantitative adhesion measures of multilayer films: Part II. Indentation of W/Cu, W/W, Cr/W

M.D. Kriese[1], N.R. Moody[2], W.W. Gerberich[1]
*([1]University of Minnesota, [2]Sandia National Laboratories)*

Sputtered copper and tungsten thin films both with and without tungsten and chromium superlayers were tested using nanoindentation probing to initiate and drive delamination. The adhesion energies of the films were calculated from the induced delaminations using the analysis presented in "Quantitative adhesion measures of multilayer films: Part I. Indentation mechanics." Copper films ranging in thickness from 150 to 1500 nm in the as-sputtered condition had measured adhesion energies ranging from 0.2 to 2 $J/m^2$, commensurate with the thermodynamic work of adhesion. Tungsten films ranging in thickness from 500 to 1000 nm in the as-sputtered condition had measured adhesion energies ranging from 5 to 15 $J/m^2$. The superlayer was shown to induce radial cracking when under residual tension, resulting in underestimation of the adhesion energy when the film was well adhered. Under conditions of weak adherence or residual compression, the superlayer provided an excellent means to induce a delamination and allowed an accurate and reasonably precise quantitative measure of thin film adhesion.

**Order No.: JA907-046** 

### Phase evolution in Ni–Nb multilayers upon solid-state reaction

G.W. Yang, C. Lin, B.X. Liu
*(Tsinghua University)*

Solid-state amorphization was achieved in the $Ni_{48}Nb_{52}$ multilayers upon thermal annealing by gradually raising the temperature from 250 °C up to

400 °C and staying at 400 °C for 2 h. More interestingly, prior to complete amorphization, a sequential disordering of first Ni and then Nb crystalline lattices was observed for the first time, and it is essentially the physical origin of an asymmetric growth of the amorphous interlayer during solid-state reaction reported previously in some binary metal systems. In another two multilayered samples with overall compositions of $Ni_{64}Nb_{36}$ and $Ni_{70}Nb_{30}$, thermal annealing under similar conditions resulted in the formation of two metastable crystalline phases with fcc and hcp structures, respectively, though an amorphous phase also appeared and co-existed with one of the metastable crystalline phases in the intermediate states. In the ion mixing experiment, such sequential disordering as well as the formation of metastable phases was also observed in the respective Ni–Nb multilayers upon room-temperature 200-keV xenon ion irradiation. Comparatively, however, ion irradiation eventually induced complete amorphization in all the multilayers at respective doses, indicating ion-induced disordering frequently predominated in the competition between amorphization and the growth of a metastable crystalline phase. A Gibbs free energy diagram, including the free energy curves of the newly formed metastable crystalline phases of the Ni–Nb system was calculated based on Miedema's model. The constructed free energy diagram can give reasonable explanations to the sequential disordering and the thermodynamic possibility of the formation of either an amorphous or metastable crystalline phase, of which the free energy difference was quite small. It follows naturally that the phase selection, namely which phase was more favored to be formed eventually than its competitors, was influenced or even determined by the kinetics involved in the respective processes.

**Order No.: JA907-047** 

## The role of the dispersed phase remnant magnetization on the redispersibility of magnetorheological fluids

P.P. Phulé, M.P. Mihalcin, S. Genc
*(University of Pittsburgh)*

The influence of the *remnant* magnetization of the soft magnetic particulates, used as a dispersed phase, on the redispersiblity of magnetorheological fluids is discussed. Calculations of the magnetic interaction energy showed that for 33 vol% MR fluids based on iron particles (~6 μm), manganese zinc ferrite fluids (~2.3 μm), and nickel zinc ferrite fluids (~2.1 μm), the ratios of the magnetic interaction energy to the thermal energy were 161000, 6400, and 3900, respectively. These calculations showed that even the seemingly small levels of remnant magnetization, associated with particulates employed in MR fluids, introduced significant dipole–dipole interparticle interactions. It is proposed that this interaction caused most MR fluids to show a tendency for "cake formation," which made it difficult to redisperse these fluids. Our modeling presented here also suggests practical strategies to enhance the redispersibility of MR fluids.

**Order No.: JA907-048** 

## Fabrication and properties of organic and metal nanocylinders in nanoporous membranes

L. Piraux, S. Dubois, J.L. Duvail, A. Radulescu, S. Demoustier-Champagne, E. Ferain, R. Legras
*(Université Catholique de Louvain)*

Chemical and electrochemical techniques were used for generating ensembles of randomly distributed organic and metal nanocylinders into the pores of nuclear track-etched polycarbonate membranes. This so-called "template method" makes possible the synthesis of a variety of materials including metals, ferromagnets, superconductors, semimetals, and conducting polymer and structures such as solid wires, tubules, composite nanostructures, and multilayers. Numerous interesting properties have been identified in relation to the nanoscopic dimensions of the materials.

**Order No.: JA907-049** 

## Oxidation kinetics of large nickel particles

R. Karmhag[1], G.A. Niklasson[1], M. Nygren[2]
*([1]Uppsala University, [2]Stockholm University)*

Oxidation of polycrystalline nickel particles with an approximate median diameter of 158 μm has been studied by thermogravimetric measurements in the temperature range 773–1473 K. The oxidation was found to be thermally activated with an apparent activation energy of about 1.9 eV at temperatures below 1073 K and 1.2 eV at higher temperatures. Our data showed the qualitative features expected for oxidation of spherical metal particles. The kinetics was compared with a homogenous field, coupled-currents theory for oxidation of spherical metal particles. Calculations using a median particle size or a distribution of particle sizes could only give a satisfactory fit to part of the experimental data. Possible explanations for the deviations in terms of space charge, grain boundary diffusion, grain growth, and sintering were discussed. Scanning electron microscopy studies of the particles after oxidation showed that there is a large difference in the surface structure and the degree of sintering between the particles oxidized at low and high temperatures.

**Order No.: JA907-050** 

## Influence of additives on the properties of spherical nickel particles prepared by ultrasonic spray pyrolysis

S. Stopić[1], J. Nedeljković[2], Z. Rakočević[2], D. Uskoković[3]
*([1]Faculty of Technology and Metallurgy, [2]Vinča Institute of Nuclear Sciences, [3]Serbian Academy of Sciences and Arts)*

Ideal spherical nonagglomerated Ni particles (mean diameter 0.62–1.12 μm) were prepared by ultrasonic spray pyrolysis of $NiCl_2$ aqueous solution in the presence of 0.1 mass% of Pd, Cu, or Ni in an $H_2$–$N_2$ atmosphere at 900 °C. Incomplete reduction of the $NiCl_2$ aqueous solution in the absence of additives was observed under the same conditions. Differential thermal and thermal-gravimetric analyses revealed a decrease in initial reduction temperature of $NiCl_2$ from 375 to 275 °C by addition of Pd, Cu, or Ni. Morphology of Ni particles was analyzed using scanning tunneling microscopy. The surface roughness of Ni particles was found to be controllable by addition of appropriate additives

**Order No.: JA907-051** 

## Magnetic properties of uniform γ–$Fe_2O_3$ nanoparticles smaller than 5 nm prepared by laser pyrolysis

M.P. Morales, S. Veintemillas-Verdaguer, C.J. Serna
*(C.S.I.C.)*

γ–$Fe_2O_3$ spherical particles with diameters between 5 and 3.5 nm—very uniform in size—have been prepared by laser pyrolysis of iron pentacarbonyl. The infrared spectra of the samples showed features that indicated different degrees of crystallinity according to the preparation conditions. Low saturation magnetization values (≈10 emu/g) and very high coercivities at low temperature (3000 Oe) have been found for the γ–$Fe_2O_3$ nanoparticles with the smallest particle size and the highest structural disorder. To explain the magnetic properties, it was necessary to consider additional anisotropies caused by the increase in surface and structural disorder as the particle size decreased.

**Order No.: JA907-052** 

## Preparation of phase homogeneous Mn–Zn ferrite powder by spray pyrolysis

X. Zhao[1], B. Zheng[1], H. Gu[1], C. Li[1], S.C. Zhang[2], P.D. Ownby[2]
*([1]East China University of Science and Technology, [2]University of Missouri—Rolla)*

Two kinds of aqueous precursor solutions were used to synthesize Mn–Zn ferrite powders: (i) Nitrate precursor (NO)—derived from solutions of $Mn(NO_3)_2$, $Zn(NO_3)_2$, and $Fe(NO_3)_3$ and (ii) Acetate precursor (AC)—derived from solutions of $Mn(CH_3COO)_2$, $Zn(CH_3COO)_2$, and $Fe(NO_3)_3$. The composition of the powders synthesized from the precursor AC was very uniform, while powders derived from the precursor NO had Mn and Zn segregated on the particle surfaces. In addition, the powders synthesized from precursor AC were solid spherical particles with fine porosity, whereas many hollow and fragmented particles were observed in the powder derived from precursor NO. Overall, the properties of Mn–Zn ferrite cores prepared from the precursor AC were superior to those prepared from the precursor NO. The reasons for the differences are explained and described in detail. The AC precursor powders synthesized by spray pyrolysis produced Mn–Zn ferrite cores with good magnetic properties.

**Order No.: JA907-053** 

## Electromechanical anisotropy behavior in $Pb_{0.88}Eu_{0.88}Ti_{1-y}Mn_yO_3$ system: Role of 90° domain reversal

O. Pérez Martínez[1], J.M. Saniger Blesa[2], A. Peláiz Barranco[3], F. Calderón Piñar[3]
*([1]Universidad de Antioquia, [2]Universidad Nacional Autónoma de México, [3]Universidad de la Habana*

An indirect observation of 90° domain reversal under the influence of poling field process was undertaken through means of x-ray diffraction study in the $Pb_{0.88}Eu_{0.88}Ti_{1-y}Mn_yO_3$ ($y$ = 0, 0.01, 0.02 and 0.03) piezoelectric anisotropic system. The optimum condition $k_p \rightarrow 0$ was achieved for $y$ = 0.02 composition. A large percentage of 90° domain rotation was necessary, but not a sufficient condition for the ultrahigh electromechanical anisotropy manifestation. A large

microstrain originated by structural defects in unpoled samples seemed to play a crucial role in the attainment of this piezoelectric anisotropy. A breaking in the translational periodicity due to induced vacancy in Pb and O sites by $Eu^{3+}$ and $Mn^{2+}$ substitutions was manifested in the nonuniform variance of the tetragonality (*c/a*), the large microstrain, and the detriment of crystallinity observed.
**Order No.: JA907-054** 

## Preparation of epitaxial $SrBi_2Nb_2O_9$ and $SrBi_2Ta_2O_9$ thin films by coating-pyrolysis process

T. Nagahama[1], T. Manabe[2], I. Yamaguchi[2], T. Kumagai[2], T. Tsuchiya[1], S. Mizuta[2]
*([1]Science University of Tokyo,*
*[2]National Institute of Materials and Chemical Research)*

Epitaxial and polycrystalline thin films of bismuth layer-structured ferroelectrics, $SrBi_2Nb_2O_9$ (SBN) and $SrBi_2Ta_2O_9$ (SBT), were prepared on single-crystal $SrTiO_3$(001) and polycrystalline yttria-stabilized zirconia substrates, respectively, by coating-pyrolysis process. The epitaxial relationship of the films and substrates was SBN, SBT (001)//$SrTiO_3$(001) and SBN, SBT [100]//$SrTiO_3$ [100], [010], where pseudotetragonal indices were adopted for SBN and SBT. The lattices of the epitaxial films were found to be slightly strained owing to stress from the substrate. Atomic force microscopy observations showed that the epitaxial films as well as polycrystalline films consisted of round-shaped, islandlike grains of submicron size.
**Order No.: JA907-055** 

## Scanning electron acoustic microscopy of electric domains in ferroelectric materials

M.L. Qian[1], X.M. Wu[1], Q.R. Yin[2], B.Y. Zhang[2], J.H. Cantrell[3]
*([1]Tongji University, [2]Chinese Academy of Sciences, [3]Langley Research Center)*

Electric domains in single-crystal and polycrystalline $BaTiO_3$ have been observed using scanning electron acoustic microscopy (SEAM). A model is presented of the SEAM signal generation, spatial resolution, and contrast mechanism associated with the imaging of electric domains in ferroelectric materials. The SEAM signal was found to depend directly on the sum of the piezoelectric coupling coefficient and spontaneous polarization of the domain, on the charge density of the electron beam interaction volume, and inversely on both the permittivity and the elastic constants of the material. Application of the model to $BaTiO_3$ yielded a contrast of roughly 3.5% from 90° domain structures and 6.8% from 180° domain structures.
**Order No.: JA907-056** 

## Synthesis, electrochemical, and microstructural study of precursor-derived $LiMn_2O_4$ powders

Y.H. Ikuhara[1], Y. Iwamoto[1], K. Kikuta[2], S. Hirano[2]
*([1]Synergy Ceramics Laboratory, [2]Nagoya University)*

Stable and homogeneous alkoxide precursor solutions of lithium ethoxyethoxide and manganese ethoxyethoxide in 2-ethoxyethanol were synthesized by ligand exchange reaction of lithium isopropoxide and manganese 2-ethoxide, respectively, with 2-ethoxyethanol. Li–Mn–O precursor solution was prepared by mixing these modified alkoxide precursor solutions. $LiMn_2O_4$ powders were successfully synthesized by the pyrolysis of the Li–Mn–O precursor powder in $O_2$ at a temperature as low as 200 °C. The nanocrystalline $LiMn_2O_4$ powders 20–50 nm in diameter after heat treatment up to 700 °C consisted of the ordered (111) plane and performed with good cyclability as the cathode materials for Li secondary batteries.
**Order No.: JA907-057** 

## Eu-doped $Y_2O_3$ phosphor films produced by electrostatic assisted chemical vapor deposition

K.L. Choy, J.P. Feist, A.L. Heyes, B. Su
*(Imperial College of Science, Technology and Medicine)*

Europium-doped yttrium oxide ($Y_2O_3$ : Eu) thermographic phosphor films were deposited on Ni-alloy substrates using a novel and cost-effective electrostatic assisted chemical vapor deposition (EACVD) technique. The thermoluminescence properties were studied under irradiation by an uv laser. It was found that crystallized $Y_2O_3$ : Eu films could be deposited at a temperature as low as 550 °C. Annealing of the as-deposited films at higher temperatures (>1000 °C) improved the luminescence properties due to further crystallization processes. The correlation of the lifetime decay and temperature change of the films showed that the EACVD-deposited films are suitable for use in phosphor thermometry for high-temperature applications.
**Order No.: JA907-058** 

## Influence of heat treatment on $LiNbO_3$ thin films prepared on Si(111) by the polymeric precursor method

V. Bouquet[1], J.A. Varela[2], E. Longo[1], E.R. Leite[1]
*([1]Universidade Federal de São Carlos, [2]Universidade Estadual Paulista)*

The effects of heat-treatment temperature on $LiNbO_3$ thin films prepared by the polymeric precursor method were investigated. The precursor solution was deposited on Si(111) substrates by dip coating. X-ray diffraction and thermal analyses revealed that the crystallization process occurred at a low temperature (420 °C) and led to films with no preferential orientation. High-temperature treatments promoted the formation of the $LiNb_3O_8$ phase. Scanning electron microscopy, coupled with EDS analyses, showed that the treatment temperature also affected the film microstructure. The surface texture—homogeneous, smooth, and pore-free at low temperature—turned into an "islandlike" microstructure for high-temperature treatments.
**Order No.: JA907-059** 

## Planar waveguides prepared by $K^+$–$Na^+$ field-assisted ion exchange in different types of silicate glass

J. Kosíková[1], J. Schröfel[2]
*([1]Academy of Sciences of the Czech Republic,*
*[2]Czech Technical University of Prague)*

The goal of this work was to address the technological problems associated with waveguide preparation by thermal- and electric-field–assisted $K^+$–$Na^+$ ion exchange in two types of soda-lime glass: common FTD and special pure GIL49. The number of modes, depth, profile, and the change in refractive index were measured for waveguides prepared at temperatures between 250 and 410 °C and electric field values between 0 and 50 V/mm. Although the influence of some admixture content inside the glass was relatively high, all of these parameters could be controlled accurately and repeatedly by the electric field.
**Order No.: JA907-060** 

## $C_{24}Cs$ samples containing oriented $N_2$ molecules

Y. Finkelstein[1,2], R. Moreh[1,2], D. Nemirovsky[1], O. Shahal[2], F. Beguin[3], L. Duclaux[3]
*([1]Ben-Gurion University, [2]Nuclear Research Center—Negev,*
*[3]CNRS-Université)*

The adsorption of $N_2$ molecules inside $C_{24}Cs$ has been studied in detail as a function of temperature and pressure using n-diffraction and nuclear resonance photon scattering (NRPS). Large differences were observed between samples derived from highly oriented pyrolytic graphite (HOPG) and those prepared from graphite powder. The tilt angle of the $N_2$ molecular axis was determined using NRPS and found to lay nearly parallel to the graphite planes. The amount of adsorbed $N_2$ increases with decreasing temperatures reaching saturation composition $C_{24}Cs(N_2)_{1.5}$ at approximately 100 K with an initial $N_2$ pressure of 2 bar. At higher pressure, 9 bar, two new phases were formed: A 2nd stage $C_{32}Cs(N_2)_{2.1}$ and a lst stage $C_{16}Cs(N_2)_{1.8}$ at $T < 170$ K and are discussed in detail.
**Order No.: JA907-061** 

## Structural mechanisms underlying near-zero thermal expansion in β-eucryptite: A combined synchrotron x-ray and neutron Rietveld analysis

H. Xu[1], P.J. Heaney[1], D.M. Yates[1], R.B. Von Dreele[2], M.A. Bourke[2]
*([1]Princeton University, [2]Los Alamos National Laboratory)*

The structures of ordered and disordered β-eucryptite have been determined from Rietveld analysis of powder synchrotron x-ray and neutron diffraction data over a temperature range of 20 to 873 K. On heating, both materials showed an expansion within the (001) plane and a contraction along the *c*-axis. However, the anisotropic character of the thermal behavior of ordered β-eucryptite was much more pronounced than that of the disordered compound; the linear expansion coefficients of the order and disordered phases were $\alpha_a = 7.26 \times 10^{-6}\ K^{-1}$; $\alpha_c = -16.35 \times 10^{-6}\ K^{-1}$ and $\alpha_a = 5.98 \times 10^{-6}\ K^{-1}$; $\alpha_c = -3.82 \times 10^{-6}\ K^{-1}$, respectively. The thermal behavior of β-eucryptite could be attributed to three interdependent processes that all caused an increase in *a* but a decrease in *c* with increasing temperature: (i) Si/Al tetrahedral deformation, (ii) Li positional disordering, and (iii) tetrahedral tilting. Because disordered β-eucryptite did not exhibit tetrahedral tilting, the absolute values of its axial thermal coefficients were smaller than those for the ordered sample. At low temperatures, both ordered and disordered β-eucryptite exhibited a continuous expansion parallel to the *c*-axis with decreasing temperature, while *a* remained approximately

unchanged. Our difference Fourier synthesis revealed localization of Li ions below room temperature, and we suggest that repulsion between Li and Al/Si inhibited contraction along the *a*-axis.
**Order No.: JA907-062** 

### Effects of carbonization atmosphere and subsequent oxidation on pore structure of carbon spheres observed by scanning tunneling microscopy

M. Inagaki[1], V. Vignal[1], H. Konno[1], A.W. Morawski[2]
*([1]Hokkaido University, [2]Technical University of Szczecin)*

The surface of carbon spheres was studied by using field-emission scanning electron microscopy and scanning tunneling microscopy (STM), paying particular attention to the effects of atmosphere during carbonization and subsequent oxidation on shape and size of the entrance of micropores. Commercial spheres of glasslike carbon prepared by carbonization of phenol resin spheres in either $N_2$ or $CO_2$ atmosphere were subjected to the oxidation by immersing into nitric acid and then heating in air at 400 °C. The size distribution of pore entrance at nanoscopic scale was determined from STM images. Carbon spheres prepared in $CO_2$ atmosphere had predominantly ultramicropores, but those prepared in $N_2$ had a very low porosity. The behavior during oxidation process in air was found to be quite different on these two carbon spheres; spheres carbonized in $N_2$ were oxidized heterogeneously, but those in $CO_2$ showed homogeneous oxidation giving a high density of ultramicropores.
**Order No.: JA907-063** 

### Thin films with nanometer-scale pillar microstructure

K. Robbie[1,2], C. Shafai[1], M.J. Brett[1]
*([1]University of Alberta, [2]Queen's University)*

Thin films possessing microstructure composed of isolated vertical pillars were deposited by glancing angle deposition (GLAD) without the need for subsequent etch processing. The GLAD technique employs substrate rotation and oblique angle flux incidence to deposit porous columnar thin film with engineered microstructures. Thin films with pillar microstructure were fabricated from a variety of metals, metal oxides and fluorides, and semiconductors. The rate and incident angle of vapor flux, as well as the substrate rotation speed during deposition, were found to critically affect pillar microstructure. Thin films with pillar diameters and densities as low as 30 nm and 3 pillars/$\mu m^2$, respectively, were deposited. The low stress, high surface area, and porous nature of these films suggests application of pillar microstructure films in optical, chemical, biological, mechanical, magnetic, and electrical applications.
**Order No.: JA907-064** 

### On the grain size and coalescence stress resulting from nucleation and growth processes during formation of polycrystalline thin films

C.V. Thompson
*(Massachusetts Institute of Technology)*

When polycrystalline films form by nucleation, growth, impingement, and coalescence of islands on a substrate surface, the grain size at impingement depends on the relative magnitudes of the nucleation rate, the growth rate, and the dimension of the zone from which adatoms diffuse to a growing island. A simple description of the interdependence of these parameters has been developed. This is used to discuss the dependence of the grain-size-at-impingement and the intrinsic stress resulting from coalescence on the deposition rate and the substrate temperature, and to discuss how these might affect texture evolution during film growth.
**Order No.: JA907-065** 

### Microtexture of shock reaction products of niobium and silica mixtures

R. Murao, M. Kikuchi, K. Fukuoka, E. Aoyagi, T. Atou, Y. Syono
*(Tohoku University)*

Shock compression experiments on powder mixtures of niobium metal and quartz were conducted for the pressure range of 30–40 GPa by a 25-mm single-stage propellant gun. Chemical reaction occurred above 35 GPa, and products were found to be mainly so-called "$Cu_3Au$-type $Nb_3Si$," which contained a small amount of oxygen. Microtextures of the specimen were examined by scanning and transmission electron microscopy. A field-emission transmission electron microscope was used for energy-dispersive x-ray analysis of microtextures in small particles found in the $SiO_2$ matrix, and various species with different Nb/Si ratio and oxygen content were shown to be produced through the nonequilibrium process of shock compression.
**Order No.: JA907-066** 







https://doi.org/10.1557/S0883769400052581 Published online by Cambridge University Press

***The 12th International Zeolite Conference was the last of the 20th century... but the proceedings of the conference are a valuable reference that will serve the zeolite science community well into the 21st century.***

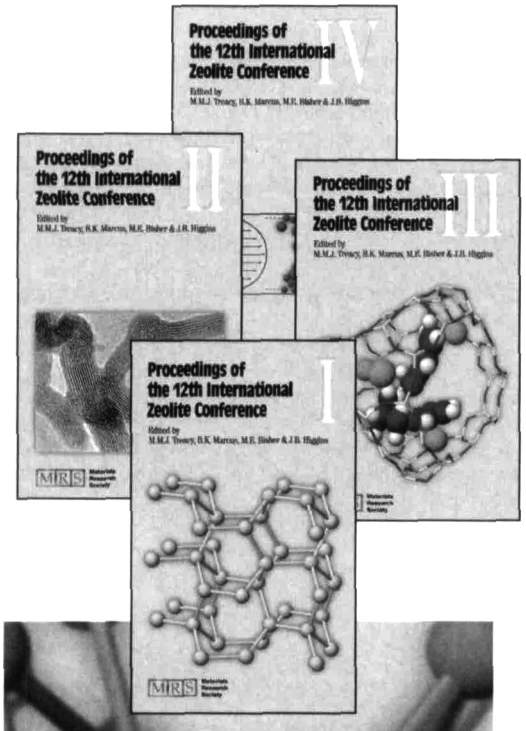


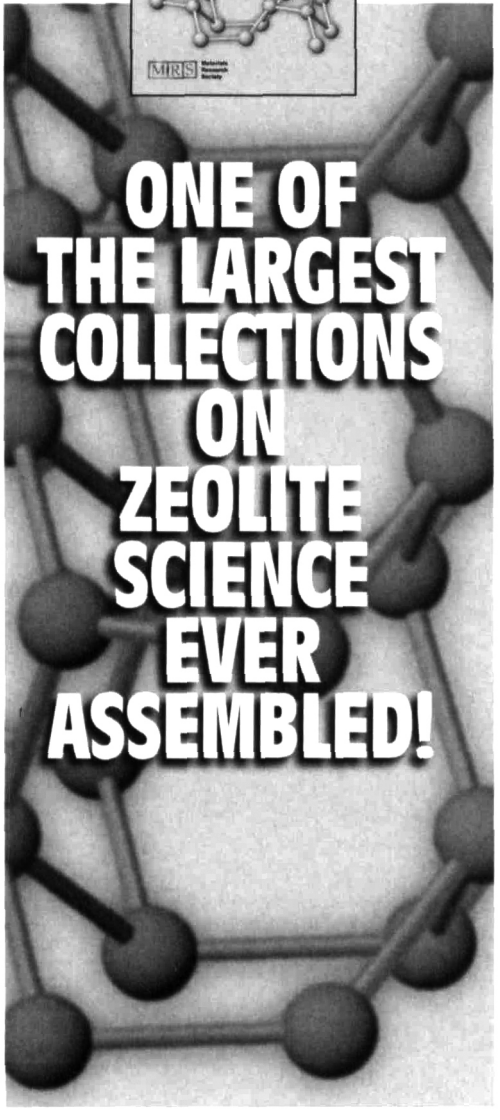


# Proceedings of the 12th International Zeolite Conference

**Editors: M.M.J. Treacy, B.K. Marcus, M.E. Bisher, J.B. Higgins**

As zeolite science continues to grow, many zeolite conferences and meetings are being held around the world, but the *premier* venue to present new work continues to be the International Zeolite Conferences. The 12th International Zeolite Conference was held in Baltimore, Maryland, in July 1998, and included 774 participants from 37 different countries. It also spawned this comprehensive four-volume, 3360-page proceedings that covers many diverse areas of zeolite study, some of which were only touched upon at previous conferences.

## Topics include:

- Diffusion
- Adsorption
- Theory and Modelling
- Structure
- Industrial Applications
- Synthesis
- Catalysis
- Membranes
- Mesoporous Materials
- Solid-State Applications
- Characterization

***For complete Table of Contents listing, check out the MRS Web site: www.mrs.org/publications/zeolite/***

1999 • Hardbound • 4 Volumes • 3360 Pages
ISBN: 1-55899-463-7 • Order Code: ZEO-B

### Proceedings of the 12th International Zeolite Conference

| | |
|---|---|
| **$220.00** | **MRS Members** |
| $245.00 | U.S. List |
| $270.00 | Non-U.S. List |

*Prices do not include shipping and handling. Select one option below.*

### Shipping/Handling Options

- U.S. Orders (shipped UPS) ..... $12.00 per 4-volume set
- Non-U.S. Orders (shipped surface) ..... $18.00 per 4-volume set
  *please allow 8-12 weeks for delivery*
- Non-U.S. Orders (shipped air freight) ..... $55.00 per 4-volume set

MRS Materials Research Society

506 Keystone Drive, Warrendale, PA 15086-7573 U.S.A. • Telephone: 724-779-3003 • Fax: 724-779-8313
E-mail: info@mrs.org • www.mrs.org/publications/books/

**Circle No. 14 on Reader Service Card.**

https://doi.org/10.1557/S0883769400052581 Published online by Cambridge University Press